ACS OMEGA

Open Access



http://pubs.acs.org/journal/acsodf

Article

# Ternary Phase-Field Simulation of Poly(vinylidene fluoride) Microporous Membrane Structures Prepared by Nonsolvent-Induced Phase Separation with Different Additives and Solvent Treatments

Zhuang Zhang, Ping Fang,* Yumeng Jiang, Shurong Cui, and Chaoyu Yang

Cite This: *ACS Omega* 2024, 9, 19911−19922

Read Online

ACCESS | Metrics & More | Article Recommendations

**ABSTRACT:** In this study, an existing ternary membrane system based on nonsolvent-induced phase separation (NIPS) with a phase-field model was optimized. To study and analyze the effects of different additives on the formation of the skin layer and the effects of the three solvents on membrane characterization under the same conditions, two-dimensional simulations of the relevant parameters of a poly(vinylidene fluoride) (PVDF) membrane system were performed. The specific application of quaternary substances in ternary membrane systems was elaborated by determining the cohesive energy density between the additives and solvents, followed by the interaction parameters $\chi$ under the joint effect of the two. The results showed that the PVDF microporous membrane formed a dense surface layer at the mass transfer exchange interface, and with an increase in the poly(ethylene glycol) (PEG) concentration, the phase separation of the skin layer was predominantly transformed from liquid−solid partitioning to liquid−liquid partitioning; the number of membrane pores increased with increasing poly(vinylpyrrolidone) (PVP) concentration. The *N*,*N*-dimethylacetamide (DMAc) solvent system had the most stable thermodynamic properties; the dimethyl sulfoxide (DMSO) solvent system had mostly large pores running through the membrane and exhibited a porous structure. Related experiments also validated the model. Therefore, this model can be applied to other PVDF ternary membrane systems to better understand the structural development of microporous PVDF membranes under different conditions.

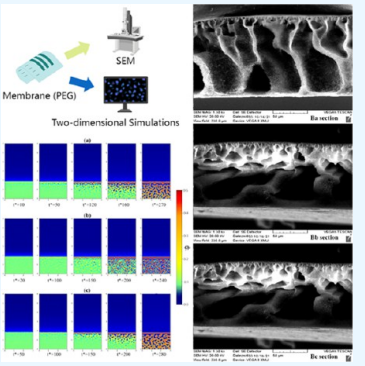


## 1. INTRODUCTION

A high-performance poly(vinylidene fluoride) (PVDF) ultrafiltration membrane can be prepared by using the nonsolvent-induced phase separation (NIPS) method. This method involves inducing solid−liquid or liquid−liquid phase separation by diffusing a certain composition of homogeneous polymer solution of solvent and nonsolvent double diffusion to change the thermodynamic instability of the polymer solution. This phase separation results in the formation of a three-dimensional subnetwork gel structure (i.e., polymer-rich phase curing), and the polymer-poor phase elutes to form a pore-like structure. The main structure of the membrane is constituted by this three-dimensional reticulated gel structure.[1] PVDF prepared using PVDF powder has good mechanical properties, weather resistance, and chemical stability and is widely used in water treatment, aerospace, biomedical, and other fields.

When NIPS is utilized for the preparation of PVDF membranes, the system mainly undergoes transient phase splitting, dominated by liquid−liquid phase splitting. The phase separation of any unit is not completed independently or instantaneously, and the rate of the interaction with the mass transfer affects the change of the content between the substances, which, in turn, also affects the membrane performance. To obtain PVDF membranes with different separation properties and perform separation efficiently, the membrane structure and the shape of the membrane pores are usually altered by varying the concentration of the casting solution, additives, solvent, and solidification temperature.[2−4] Dense skin is formed by gels, and porous skin is formed by liquid−liquid phase separation.[5] Additives, as pore-making agents, have an important influence on the membrane skin structure, whereas different solvent systems have different degrees of influence on the membrane structure and properties. The phase-field method can introduce field variables (usually component local volume fractions), specifically study the polymer melt and solution phase-separation process, and can be used to characterize the local composition

Received: November 21, 2023
Revised: April 8, 2024
Accepted: April 10, 2024
Published: April 24, 2024

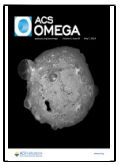

at various locations in the phase region and changes at the interface of the two-phase regions.

Flory−Huggins' thermodynamic theory suggests that a number of kinetic models can be employed, such as the microscale phase-field theory and microscale molecular/particle-based simulation methods. To date, several experimental and simulation studies of the phase-separation process and simulation structures have been conducted with different control factors in the film formation process. The initial study of NIPS modeling involved a one-dimensional steady-state diffusion model developed by Cohen et al.[6] in 1979. In 1988, McHugh et al.[7,8] constructed a pseudobicomponent model based on the phase-separation behavior of a polymer/solvent/nonsolvent ternary system. In addition, Cheng et al.[9] benefited from the experience of the previous model and demonstrated the formation and numerical prediction of various membrane structures. Zhou et al. extended the simulation to two and three dimensions, such that the simulated system was a nonsolvent/solvent/polymer ternary system with periodic boundary conditions and homogeneous initial conditions, and the formation of the asymmetric phase-separation morphology induced by interphase mass transfer was characterized by simulation.[10] Zhang et al.[11] investigated the intermolecular forces between additives, solvents, and inorganic agents and their effects on membrane structure and properties using density functional theory (DFT). However, the existing models do not systematically consider the effects of additives in conjunction with the solvents. The main objective of this study was to establish a quaternary substance phase-field model based on the kinetic theory of polymer macromolecules by applying the ternary Cahn-Hillard equation and the Flory−Huggins thermodynamic theory. The membrane structure was examined under different additive and solvent conditions to elucidate the process of the development of membrane structures under different conditions.

In this study, the dimensionless and three boundary conditions are specified based on the phase-field model. The quaternary substance is processed by utilizing a ternary system, combining the additives and solvents into a single whole, and readjusting the parameters of the thermodynamic system to conform to the quaternary solution to improve the applicability of the model. The effects of additives on skin formation and three different solvents on membrane characterization under the same conditions are presented by combining experiments and phase-field simulations and compared to the experimental results to verify the correctness of the model. The differences in the PVDF membrane structure are also revealed in the final form with different additives and solvents.

## 2. MODEL

The initial diffusion and phase separation are two different phenomena. During submergence, diffusion eliminates the differences in the concentrations of the substances. During phase separation, the concentration of the substance undergoes an "uphill" phenomenon, which leads to a larger concentration difference between different substances. Because the change in concentration between substances is driven by the minimum free energy between regions, the free energy is described by the phase-field model.

The phase-field approach is based on the Ginzburg−Landau theory, which describes the occurrence of phase transitions in substances. Differential equations are used to reflect the diffusion processes, changes in chemical potentials, and thermodynamic driving forces associated with specific physical mechanisms. The development of phase-field modeling began in the 1950s and continued aggressively in the 1970s. Kahn, Hilliard, and Allen proposed nonzero-thickness diffusion between separated phases based on a study involving spinodal dynamics. In this study, based on the Flory−Huggins theory, when only binary interactions between the substances are considered to occur, the Gibbs free energy of mixing for a ternary solution system containing a polymer is expressed as[12−15]

$$\frac{\Delta G}{RT} = \left[\varphi_n \ln \varphi_n + \varphi_s \ln \varphi_s + \frac{\varphi_p}{m_p}\ln \varphi_p + \chi_{ns}\varphi_n\varphi_s + \chi_{sp}\varphi_s\varphi_p + \chi_{np}\varphi_n\varphi_p\right] \times (n_n + n_s + m_p n_p) \quad (1)$$

where $R$ is the gas constant, $T$ is the temperature, $n_i$ and $\varphi_i$ are the mole number and volume fraction of component $i$, respectively, and $\chi_{ij}$ is the Flory−Huggins interaction parameter ($i,j = p,s,n$, where the component $n$ is the nonsolvent, $s$ is the solvent, and $p$ is the polymer).

Because the quaternary system is more complex and difficult to solve by finite volume, the quaternary substance is treated using the ternary system, the solvent and the additive are viewed as a whole, denoted by $s$-$q$, and the parameters of the thermodynamic system are readjusted so that it conforms to the quaternary system. In the Flory−Huggins thermodynamic model, the interaction parameter $\chi_{ij}$ ($i,j = p,s,n,s$-$q$) is the most important, and it can be used as an important index to judge the compatibility between substances. For the polymer $n$ mixed system with solvent and additive molecules $s$-$q$, $\chi_{n(s\text{-}q)}$ can be calculated from the mixing energy $\Delta E_{mix}$, as follows:

$$\chi_{n(s\text{-}q)} = \left(\frac{\Delta E_{mix}}{RT}\right)V_{mon} \quad (2)$$

where $R$ is the gas constant, $T$ is the simulation temperature, and $V_{mon}$ is the average molar volume of the monomer, which can be obtained by dividing the volume of the mixed system by the number of repeating units. Table 1 shows the specific values of $\chi$ at different volume fractions for each system.

**Table 1. Parameters of Flory-Huggins Interactions in the System ($\chi_{ij}$)**

| systems | volume fraction (%) | $\chi_{n(s\text{-}q)}$ | $\chi_{(s\text{-}q)p}$ | $\chi_{np}$ |
|---|---|---|---|---|
| PEG/PVDF/DMF/$H_2O$ | 5/18/72/5 | 0.22 | 0.17 | 0.97 |
| | 10/18/67/5 | 0.24 | 0.17 | 0.98 |
| | 15/18/62/5 | 0.21 | 0.18 | 0.97 |
| PVP/PVDF/DMF/$H_2O$ | 2/18/75/5 | 0.33 | 0.21 | 0.82 |
| | 5/18/72/5 | 0.35 | 0.21 | 0.81 |
| | 10/18/67/5 | 0.33 | 0.22 | 0.84 |

When the mixed system reaches equilibrium, the mixing energy $\Delta E_{mix}$ is given by

$$\Delta E_{mix} = \phi_n\left(\frac{E_{coh}}{V}\right)_n + \phi_{s\text{-}q}\left(\frac{E_{coh}}{V}\right)_{s\text{-}q} - \left(\frac{E_{coh}}{V}\right)_{mix} \quad (3)$$

where $\phi_n$ and $\phi_{s\text{-}q}$ are the volume fractions of components $n$ and $s$-$q$, respectively. The terms in parentheses are the cohesive energy densities of the components $n$, $s$-$q$, and the mixed system.



https://doi.org/10.1021/acsomega.3c09274
ACS Omega 2024, 9, 19911−19922

However, the phase is uniquely determined by the values of the conserved field variables (e.g., concentration and volume fraction), that is the conserved Ginsberg–Landau equation, which is a diffusion equation derived from the total free energy equation of the system.

The tissue evolution of a ternary PVDF membrane system can be characterized in terms of binary volume fractions (i.e., $\varphi_p$ and $\varphi_s$), and the spatial evolution of the system can be obtained by solving the generalized Cahn–Hilliard diffusion equation[16] as follows:

$$\frac{\partial \varphi_p}{\partial t} = -\nabla J_p + \zeta \tag{4}$$

$$\frac{\partial \varphi_{s\text{-}q}}{\partial t} = -\nabla J_{s\text{-}q} + \zeta \tag{5}$$

where $\zeta$ is the thermal noise term described by $\zeta^2 = \langle(\partial\varphi)^2\rangle$, and is the mean square deviation of the component, i.e., the intensity of fluctuations.[17] $J_i$ is the diffusive flux of component $i$. Based on the nonequilibrium thermodynamic theory proposed by Onsager et al.,[18] it can be described by the chemical mobility and chemical potential gradient equations as follows:

$$J_p = -M_{pp}\nabla(\mu_p - \mu_n) - M_{p(s-q)}\nabla(\mu_{(s-q)} - \mu_n) \tag{6}$$

$$J_{s\text{-}q} = -M_{(s\text{-}q)(s\text{-}q)}\nabla(\mu_{s\text{-}q} - \mu_n) - M_{p(s\text{-}q)}\nabla(\mu_p - \mu_n) \tag{7}$$

where $\mu_{s\text{-}q}$, $\mu_p$, and $\mu_n$ are the chemical potentials of the components $s$-$q$, $p$, and $n$, respectively. $M_{ii}$ is chemical mobility, which is closely related to the self-diffusion coefficient $D_i$:[19]

$$M_{pp} = \frac{D_p}{\frac{\partial^2 f}{\partial \varphi_p^2}} \tag{8}$$

$$M_{(s\text{-}q)(s\text{-}q)} = \frac{D_{s\text{-}q}}{\frac{\partial^2 f}{\partial \varphi_{s\text{-}q}^2}} \tag{9}$$

where $f$ is the body free energy density (unit molar free energy).

It is obtained according to eq 1:

$$f = \frac{RT}{V_m}\left(\varphi_n \ln \varphi_n + \varphi_{s\text{-}q}\ln \varphi_{s\text{-}q} + \frac{\varphi_p}{m_p}\ln \varphi_p + \chi_m \varphi_n \varphi_{s\text{-}q} + \chi_{(s\text{-}q)p}\varphi_{(s\text{-}q)}\varphi_p + \chi_{np}\varphi_n\varphi_p\right) \tag{10}$$

According to the Stokes–Einstein equation,[20−22] the diffusion coefficient is expressed as

$$D = \frac{K_b T}{\eta} \tag{11}$$

where $D$ is the diffusion coefficient of the substance, $K_b$ is the Boltzmann constant, and $\eta$ is the viscosity of the liquid.

The difference $(\mu_i - \mu_j)$ between the chemical potentials of the substances is equal to the variance of the total local free energy $G$ over the local volume fraction $\varphi_i$ as follows:

$$\frac{\delta G}{\delta \varphi_p} = (\mu_p - \mu_n) \tag{12}$$

$$\frac{\delta G}{\delta \varphi_{(s\text{-}q)}} = (\mu_{(s\text{-}q)} - \mu_n) \tag{13}$$

According to Zhou et al.,[10] eqs 9 and 10 can be written as

$$\mu_p - \mu_n = \frac{\delta f}{\delta \varphi_p} - K_{pp}\nabla^2\varphi_p - \frac{1}{2}(K_{(s\text{-}q)p} + K_{p(s\text{-}q)})\nabla^2\varphi_{(s\text{-}q)} \tag{14}$$

$$\mu_{s\text{-}q} - \mu_n = \frac{\delta f}{\delta \varphi_{s\text{-}q}} - K_{(s\text{-}q)(s\text{-}q)}\nabla^2\varphi_s - \frac{1}{2}(K_{(s\text{-}q)p} + K_{p(s\text{-}q)}\nabla^2\varphi_{(p\text{-}q)} \tag{15}$$

where $K_{ij}$ is the gradient penalty coefficient.

Because of the actual processes of substance immersion and precipitation, an additional boundary condition was added to make the simulation results more consistent with the actual situation. To establish the periodic boundary condition, the entire unit was disassembled into individual physical units with spatiotemporal periodicity for processing; thus, weakening the boundary effect.[23] The use of periodic boundary conditions causes the chemical potential $(\mu)$ and the volume fraction of matter $(\varphi_i)$ to repeat in each direction.

The substance should cause movement out of the plane of symmetry and rotation in the plane of symmetry in one direction. Therefore, the displacement along the normal to the line of symmetry, the angle of rotation around the line of symmetry, the displacement along the line of symmetry, and the angle of rotation in the modeling plane were set to zero. As the polymer solution was located at the base of the gel bath, the interface was chosen as a symmetric boundary.[24] In the simulation, the symmetric boundary condition was expressed as follows:

$$\left.\frac{\partial \varphi_i}{\partial y}\right|_y = 0 \tag{16}$$

$$\left.\frac{\partial \mu_i}{\partial y}\right|_y = 0 \tag{17}$$

The two basic forms of mass transfer caused by the irregular motion of molecules are called molecular diffusion.[25,26] Mass transfer caused by concentration differences is called convective diffusion.[27,28] Therefore, to better conform the model to the actual membrane formation process, a mass-transfer boundary condition at the top of the simulation domain, that is, molecular diffusion, was proposed. In the $X$ and $Z$ directions, the mobility $(M_{ij})$ and chemical potential $(\mu_i)$ are expressed as

$$J_{ix} = -M_{ij}\frac{\partial \mu_i}{\partial x} - M_{ij}\frac{\partial \mu_j}{\partial x} \tag{18}$$

$$J_{iz} = -M_{ii}\frac{\partial \mu_i}{\partial z} - M_{ij}\frac{\partial \mu_j}{\partial z} \tag{19}$$

where $J_{ix}$ is the scattering of the substance in the $x$-direction and $J_{iz}$ is the scattering of the substance in the $z$-direction.

The second boundary condition at the additional boundary is



https://doi.org/10.1021/acsomega.3c09274
ACS Omega 2024, 9, 19911−19922

$$\frac{\partial^2 \varphi_i}{\partial y^2} = 0 \tag{20}$$

Since the symmetry of the laws of physics implies the invariance of the laws of physics, the laws of physics have to be expressed in dimensionless form.[29−31] Although the dimensionless form has not been sufficiently analyzed in previous studies, this experiment simplifies the calculations using dimensionless equations, which profoundly reflect the intrinsic variations in physics.

After dimensionalizing the equations based on the simulated length and time, the expressions are as follows

$$\tilde{r} = \frac{r}{L} \tag{21}$$

$$\tilde{t} = \frac{t}{\bar{t}} = \frac{t}{\frac{L^2 v}{M_{pp} RT \langle \psi^n \rangle}} \tag{22}$$

where $L$ is the length of the simulation area and $\tilde{t}$ is the characteristic diffusion time scale of the polymer.

The control equation can be derived as follows:

$$\frac{\partial \varphi_p}{\partial t} = \nabla \left[ \frac{D_p}{\frac{\partial^2 f}{\partial \varphi_p^2}} \nabla \left( \frac{\delta f}{\delta \varphi_p} - K_p \nabla^2 \varphi_p - \frac{1}{2}(K_p + K_{p(s\text{-}q)}) \nabla^2 \varphi_{(s\text{-}q)} \right) \right] + \zeta \tag{23}$$

$$\frac{\partial \varphi_{s\text{-}q}}{\partial t} = \nabla \left[ \frac{D_{s\text{-}q}}{\frac{\partial^2 f}{\partial \varphi_{s\text{-}q}^2}} \nabla \left( \frac{\delta f}{\delta \varphi_{s\text{-}q}} - K_{s\text{-}q} \nabla^2 \varphi_{s\text{-}q} - \frac{1}{2}(K_p + K_{p(s\text{-}q)}) \nabla^2 \varphi_\rho \right) \right] + \zeta \tag{24}$$

## 3. EXPERIMENTAL SECTION

**3.1. Materials and Reagents.** Analytically pure reagents dimethyl sulfoxide (DMSO), *N*,*N*-dimethylacetamide (DMAc), and *N*,*N*-dimethylformamide (DMF) were purchased from Tianjin Komeo Chemical Reagent Co. Analytically pure poly(ethylene glycol) 1000 (PEG) and poly(vinylpyrrolidone) K30 (PVP) were purchased from Tianjin Chemical Reagent Co. PVDF (FR904) was purchased from Shanghai San Aifu New Materials Co. Deionized water was used as the nonsolvent.

The parameters of the additives and solvents are summarized in Table 2.

**3.2. Preparation of PVDF Flat Microporous Membranes.** To assess the accuracy of the model, we divided the experiment into five groups, assuming that the variables in each group were unique, as shown in Table 3.

Prior to the experiment, PVDF (18%) was dried in an oven at 60 °C for 24 h to remove excess water. The solvent and deionized water were added to a conical flask in an appropriate ratio (10:1) and dispersed by sonication. An amount of PVDF was weighed and placed into the mixture according to the grouping to obtain the desired 0.10, 0.15, and 0.20 volume fractions of the different solvents DMSO, DMAc, and DMF and stirred at 60 °C for 10 h until it was completely dissolved. The mixture was kept in a 60 °C water bath for 12 h for defoaming. Next, the casting solution was poured onto a glass plate and scraped with a spatula to make a solution film (chosen to be 200 $\mu$m thick), which was quickly immersed in a pure aqueous solution at room temperature for the phase transition. The water was changed every 8 h during the first 3 days (72 h) and daily for the following 4 days. After 7 days, the phase transformation of the membranes was considered complete, and the membranes were stored in pure water for later use. The solvent used for the additive control was DMF; the additives were placed in weighed PVDF and mixed with it, and the rest of the membrane formation process was the same as described above.

**Table 2. Parameters of the Chemical Compound**

| chemical name | chemical formula | CAS number | densities (g/cm$^3$) |
|---|---|---|---|
| $H_2O$ | $H_2O$ | 7732−18−5 | 1 |
| PVDF | $-(C_2H_2F_2)_n-$ | 24937−79−9 | 1.77 |
| PVP | $(C_6H_9NO)_n$ | 9003−39−8 | 1.69 |
| PEG1000 | $HO(CH_2CH_2O)_nH$ | 25322−68−3 | 1.125 |
| DMSO | $C_2H_6OS$ | 67−68−5 | 1.100 |
| DMAc | $C_4H_9NO$ | 127−19−5 | 0.937 |
| DMF | $C_3H_7NO$ | 68−12−2 | 0.945 |

**Table 3. Ratios for Each Group**

| case | PVDF (wt %) | solvents | additive (wt %) | gelatin bath | temperature $T$ (K) |
|---|---|---|---|---|---|
| Aa | 18 | DMF | | purified water | 333.15 |
| Ab | 18 | DMSO | | purified water | 333.15 |
| Ac | 18 | DMAc | | purified water | 333.15 |
| Ba | 18 | DMF | PEG (5%) | purified water | 333.15 |
| Bb | 18 | DMF | PEG (10%) | purified water | 333.15 |
| Bc | 18 | DMF | PEG (15%) | purified water | 333.15 |
| Ca | 18 | DMF | PVP (2%) | purified water | 333.15 |
| Cb | 18 | DMF | PVP (5%) | purified water | 333.15 |
| Cc | 18 | DMF | PVP (10%) | purified water | 333.15 |

**3.3. Characterization of PVDF Membranes.** The crystal structures and crystallinities of the membranes were characterized by using a wide-angle X-ray diffractometer (Rigaku, Dnax-rA). The morphology and structure of the top and bottom surfaces as well as the end faces of the membranes were characterized by using field-emission scanning electron microscopy (SEM, DSa 100, Hitachi, Japan). The porosity was determined by using wet and dry specific gravity methods. The specific steps were as follows: the pure membrane was cut into 2 cm × 2 cm samples, the water droplets on the surface were wiped off with filter paper, the weight of the sample was recorded, the sample was dried, and the weight of the sample was recorded. Each membrane was tested thrice, the mean value was calculated, and the porosity of the membrane ($\varepsilon_0$) was determined using equation


https://doi.org/10.1021/acsomega.3c09274
ACS Omega 2024, 9, 19911−19922

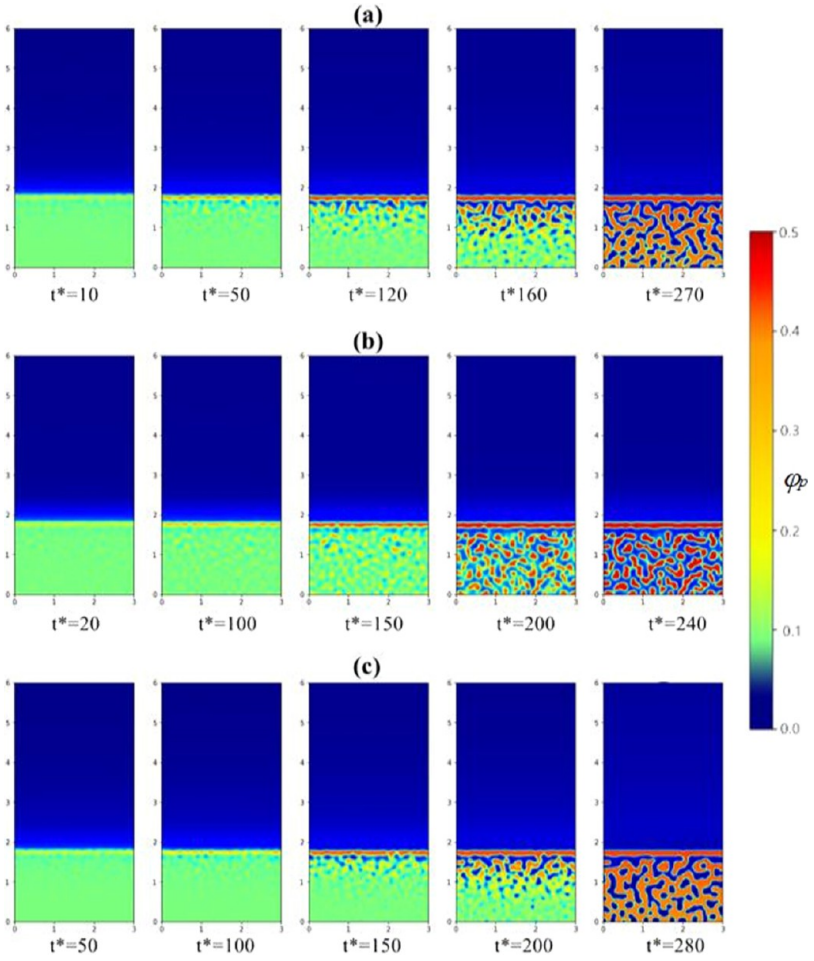


**Figure 1.** Microscopic simulation of the quaternary PVDF membrane system under different PEG concentrations (a–c) at different times.

$\varepsilon_0 = \frac{(m_s - m_g)/\rho_w}{(m_s - m_g)/\rho_w + m_g/\rho_p} \times 100\%$. In this study, the average pore size of the membrane $r_m$ was obtained using filtration velocimetry based on the Guerout Elford–Ferry formula: $r_m = \sqrt{\frac{(2.9 - 1.75\varepsilon) \times 8\eta l Q}{\varepsilon_0 \cdot A \cdot \Delta P}}$, where $\varepsilon_0$ is the porosity of the membrane (%), $\eta$ is the viscosity of the water, $8.9 \times 10^{-4}$ Pa·s, $l$ is the thickness of the membrane (m), $Q$ is the volume of filtered water per unit time ($m^3/s$), $A$ is the effective area of the membrane ($m^2$), and $\Delta P$ is the operating pressure (MPa). The crystallinity was calculated by the differential scanning calorimetry (DSC) method using the formula: $X_c = \frac{\Delta H_m}{\Delta H_m^0} \times 100\%$, where $H_m$ and $\Delta H_m^0$ are the melt baking of the measured sample and the melt baking of the 100% crystalline sample, respectively, and $\Delta H_m^0$ of PVDF is 104 j·g.[32,33]

## 4. RESULTS AND DISCUSSION

Anaconda 3.0 program was used to solve the equations. The gradient cross-penalty coefficients $K_{ss} = K_{pp} = K_{qq}$ were used to perform simulations, and the values of $K_{ss}$ and $K_{pp}$ were determined using the constants derived by Caneba et al.[34] During the calculations, the area of the two-dimensional (2D) simulation was chosen to be $3 \times 6\ \mu m^2$ to ensure that the ratio of the $x$-dimension to the y-dimension was 1:2. A resolution of 200 × 400 pixels was used as the analytical grid. The simulation applied a combination of 30% film-forming liquid and a 70% gel bath. Because the amount of residual polymer and solvent in the nonsolvent is small, a neutralization value of 0.01 was assumed in the gel bath.

In Section 4.1, simulations of the effects of different concentrations of different additives on the surface structure of the PVDF membrane are presented. The effects of different solvents on the structure and properties of the PVDF membranes are discussed in Section 4.2.

**4.1. Effect of Different Additives at Different Concentrations on the Structure of the Cortex.** Additives are used as the fourth component, which can improve the structure and properties of the membrane. Herein, additives are added to the casting solution. In initial studies, additives were mainly used to create more holes in the membrane, and at this time, they were also referred to as pore makers.[35−42] However, an increasing number of studies have found that the role of additives is different in different cast-film fluid systems; that is, additives can either inhibit the formation of macropores or lead to the formation of macropores. For example, Muyake et al. investigated the inhibitory effect of PEG on macropore formation when added to a cast film fluid, and Han et al. found that different molecular weights and concentrations of additives used in PVP could promote the development and inhibition of macroporosity.[43,44]

Therefore, to study the effect of different additive concentrations on the evolution of the cortical structure, different concentrations of the two additives were selected for


https://doi.org/10.1021/acsomega.3c09274
ACS Omega 2024, 9, 19911−19922

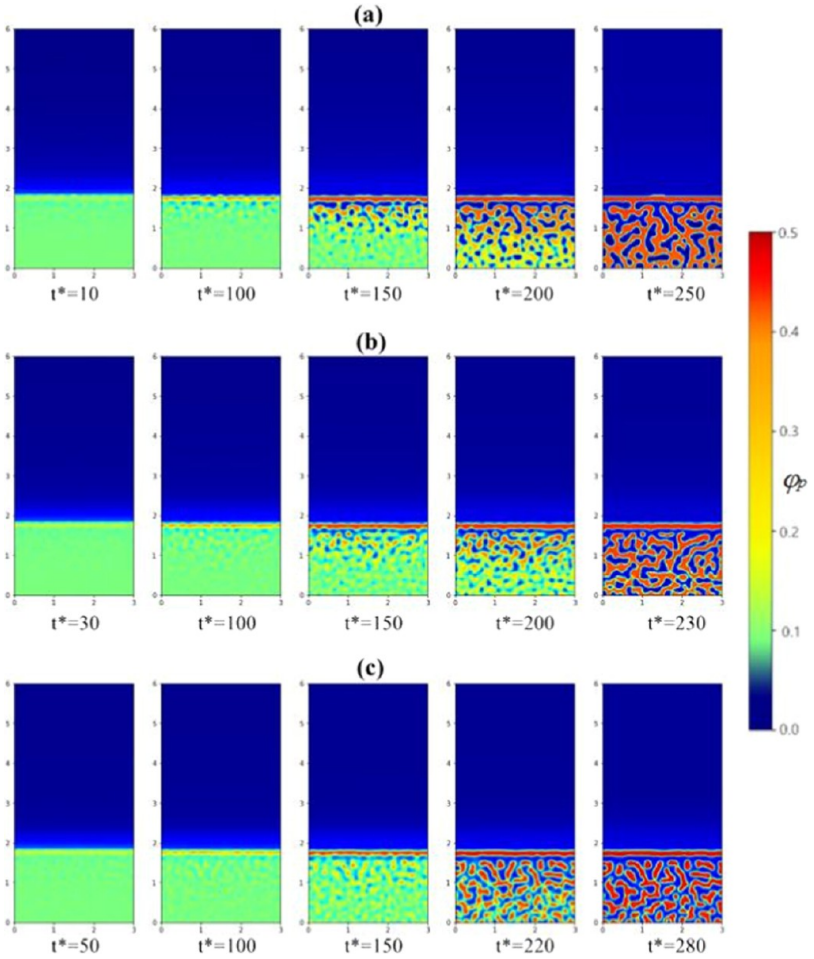


**Figure 2.** Microscopic simulation of the quaternary PVDF membrane system under different PVP concentrations (a−c) at different times.

simulations under the same conditions. Figure 1 shows the microsimulation at different PEG concentrations (a, 5%; b, 10%; c, 15%) when the volume fraction of PVDF is 18%. Figure 2 shows the microsimulation at different PVP (a, 2%; b, 5%; c, 10%) when the volume fraction of PVDF is 18%. Figure 3 shows the SEM images at different PEG concentrations (a, 5%; b, 10%; c, 15%) when the volume fraction of PVDF is 18%. Figure 4 shows the SEM images at different PVP (a, 2%; b, 5%; c, 10%) when the volume fraction of PVDF is 18%. Figures 5 and 6 show the trend between the porosity and film formation time at different concentrations of different additives.

From the data and image representations of the experimental results and the results of the simulated micrographs of the variations, it can be analyzed that the simulated micrographs of the variations are consistent with the experimental electron microscopy graphs. The experimental and simulation results show that the upper surface of the membrane exhibits a structure dominated by the liquid−solid split phase, and with the increase in the PEG concentration in the casting solution, the phase separation of the skin layer is transformed from the liquid−solid split phase to the liquid−liquid split phase dominated by the liquid−liquid split phase. The simulation results show that with an increase in the PEG concentration, the delayed skin layer time increases and the cortex becomes thicker and denser. According to Fang et al.,[45,46] a PVDF concentration of 18 wt % has a dense cortex and produces a dense granular phase, which leads to an increase in the concentration of the casting liquid. The liquid−solid phase is more likely to occur after the addition of PEG, so the porous structure caused by liquid−liquid phase separation does not exist. Therefore, the pores on the membrane surface are caused by the migration of PEG in the late stage of membrane formation. The molecular weight of PEG is very large, and it migrates into the poor polymer phase nucleus during precipitation. As can be seen from Table 4, the water flux, porosity, average pore size, and crystallinity of the membrane are maximum at a PEG concentration of 10 wt %, and the membrane physical properties and membrane morphology are optimized at this time. The simulation results show that the addition of PEG increases the viscosity of the entire system and the increase in viscosity hinders mass transfer and exchange between the components. This leads to a slower sedimentation rate of the cast film solution. However, the volume and pore size of PEG increase owing to the increase in PEG concentration; however, when the viscosity of the casting liquid increases to a certain value, owing to the rise in the system viscosity, more PEG is left in the membrane, which is ultimately larger than that diffused into the solidification bath during the precipitation process. This results in a denser membrane surface, making a portion of the PEG unable to precipitate out, resulting in the formation of a surface with a small pore size.

In this study, we analyzed the film-forming mechanism of PVP based on the study of PEG. The membrane formation mechanism of PVP is similar to that of PEG as an additive.



https://doi.org/10.1021/acsomega.3c09274
ACS Omega 2024, 9, 19911−19922

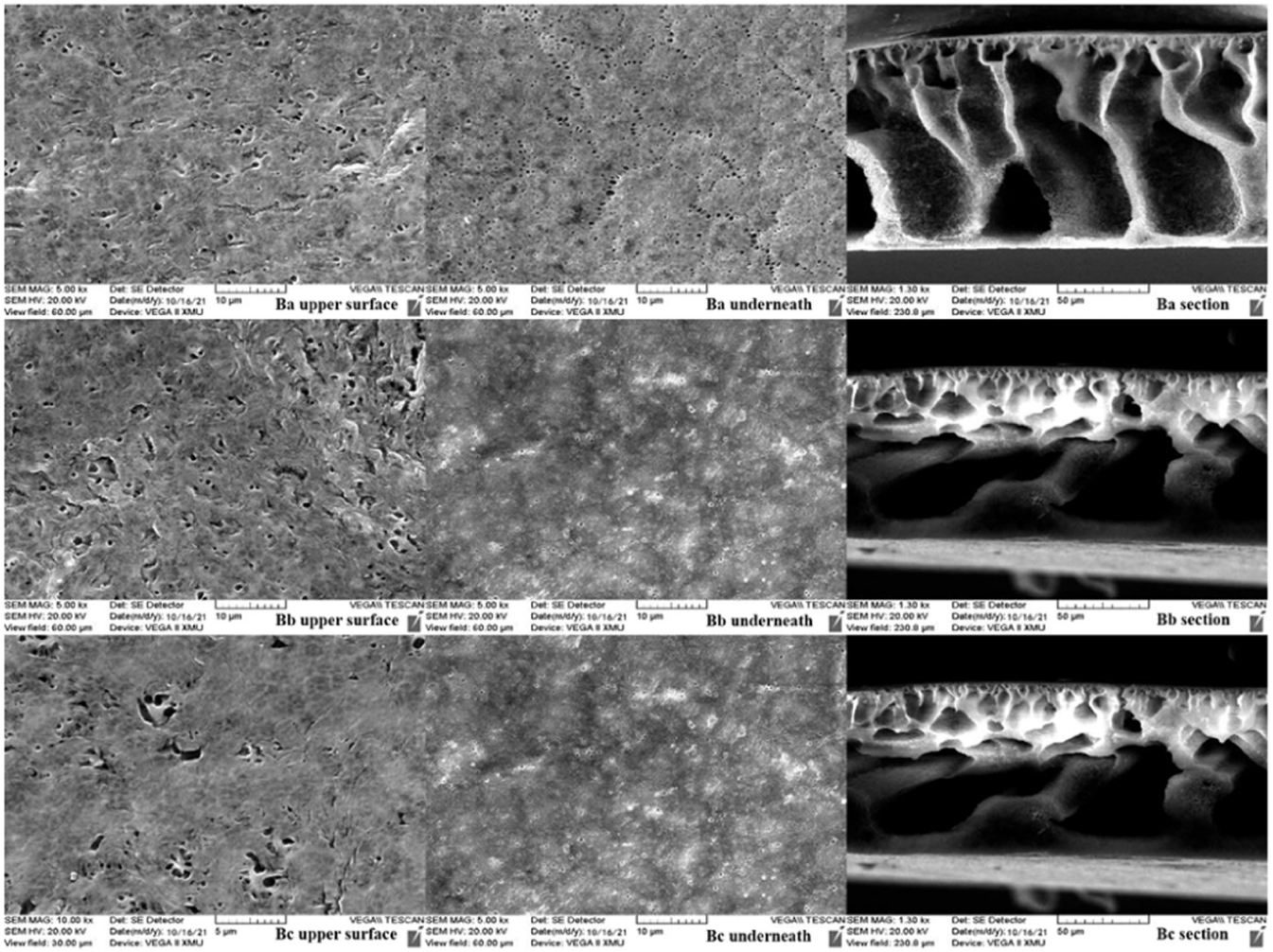


**Figure 3.** Electron microscopy images of PVDF membranes with different PEG concentrations.

However, because of the slower formation, the PVDF crystals grow into flakes of smaller diameter and higher thickness under certain conditions. There are two stages of skin formation: the precipitation stage (15 min) and the blister film stage (6−7 days). In the precipitation stage, the skin-casting solution undergoes liquid−solid phase separation and PVP diffuses into the solidification bath with the solvent DMAc during the phase-separation process. The molecular weight of PVP is much larger than that of DMAc and the nonsolvent ($H_2O$), and PVP forms its own nucleus in the interstitial space of the PVDF nuclei without complete diffusion into the solidification bath, that is, PVP is a crystalline polymer with its own crystalline nucleus. With an increase in the PVP concentration, the crystallinity of the membrane decreases, the thickness of the membrane does not change significantly, and the porosity and average pore size first increase and then decrease. Therefore, the formation of the membrane skin layer has different characteristics according to different concentrations of PVP. On the one hand, with the increase in PVP concentration, the delayed liquid−solid partitioning phase dominates the formation of the membrane, reduces the precipitation rate, and prolongs the delay time. On the other hand, the formation of the PVP surface is dense, and most of the crystalline aggregates of the PVP are left on the surface of the membrane and the incipient membrane, but when the concentration of PVP is high (e.g., 10 wt %) because of the high viscosity of the whole system, the entanglement of the PVP and PVDF chains increases and the migration decreases. The second stage of membrane surface formation is the blistering stage, where water immersion causes the PVP to gather on the membrane surface, further dissolving out and forming holes on the membrane surface. With an increase in the PVP concentration, the membrane surface holes also increase gradually. However, when the PVP concentration rises to a certain value (10 wt %), the PVP diffused into the coagulation bath by the precipitation process reduces, and those that are left in the membrane increase, ultimately resulting in a reduction in the number of pores in the membrane skin layer and pore diameter. The vesicle stage, the second stage of membrane surface formation, leads to the accumulation of PVP on the membrane surface for further dissolution. As the concentration of PVP increases, its volume also increases and the number of PVP pores on the membrane increases. However, as the PVP concentration increases to a certain value, the number and size of the membrane pores decrease because of the precipitation, which diffuses less into the coagulation bath and leaves more PVP inside the membrane.

**4.2. Effect of Different Solvents on the Membrane Structure and Properties.** To investigate the effect of the solvent type on the morphological and structural changes of the membrane and to elucidate the changes in the membrane



https://doi.org/10.1021/acsomega.3c09274
*ACS Omega* 2024, 9, 19911−19922

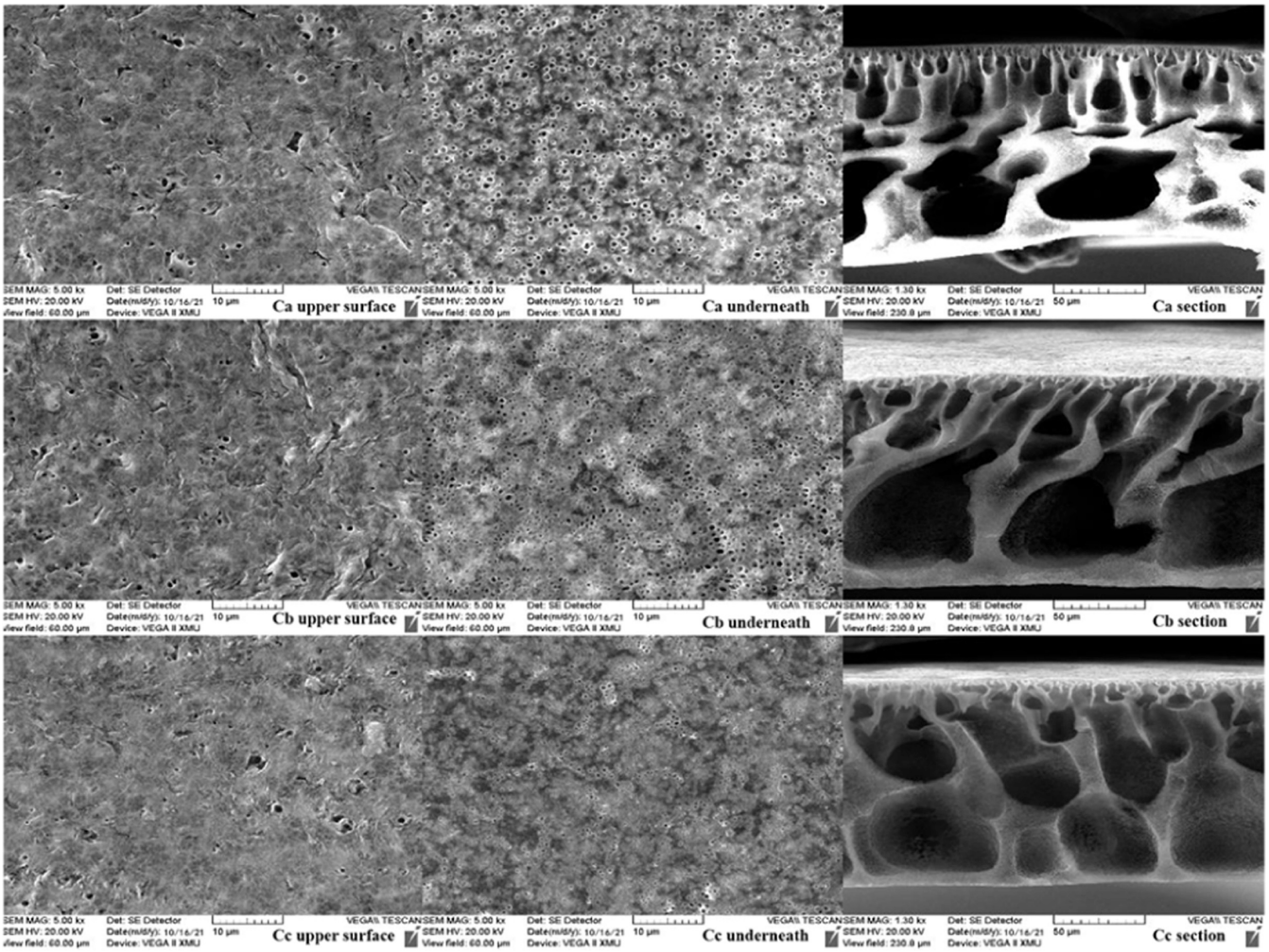


**Figure 4.** Electron microscopy images of PVDF membranes with different PVP concentrations.

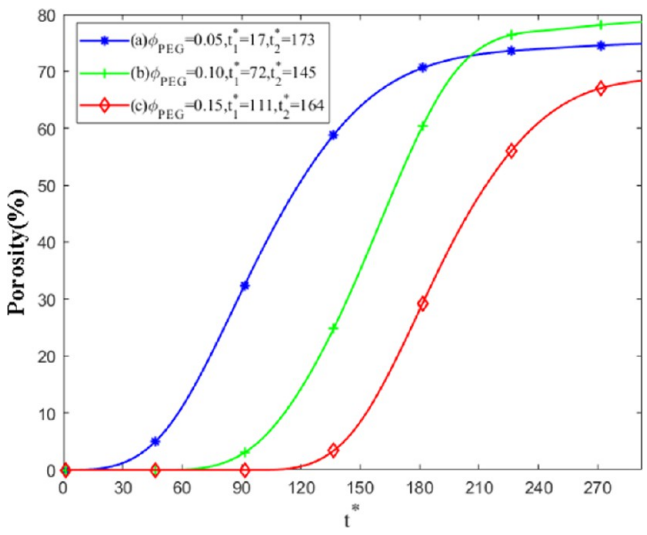


**Figure 5.** Trends of porosity and time required for film formation in systems with different PEG concentrations during simulations.

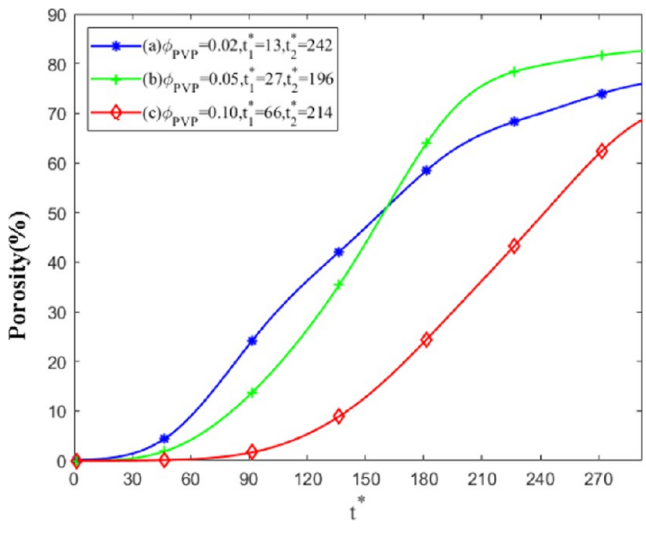


**Figure 6.** Trends of porosity and time required for film formation in the system with different PVP concentrations during simulations.

structure, we fixed the initial PVDF volume fraction at 18% for the analytical study. Figure 7 shows the microsimulation under different solvents (a, DMF; b, DMAc; c, DMSO) when the volume fraction of PVDF is 18%. Figure 8 shows the SEM images under different solvents (a, DMF; b, DMAc; c, DMSO) when the volume fraction of PVDF is 18%.

Based on the simulations in Figure 7, we can see that the size of the membrane pores and the final appearance of the membrane cortex differ for different solvents. The membrane



https://doi.org/10.1021/acsomega.3c09274
ACS Omega 2024, 9, 19911−19922

**Table 4. Properties of Membranes with Different PEG and PVP Concentrations**

| serial number | film thickness (nm) | water flux ($L \cdot m^{-2} \cdot h^{-1}$) | porosity (%) | average pore size (nm) | crystallinity (%) |
|---|---|---|---|---|---|
| Ba | 66.3 | 350.95 | 83.4 | 12.31 | 22.9 |
| Bb | 67.8 | 380.22 | 84.6 | 24.53 | 25.6 |
| Bc | 68.6 | 212.27 | 78.1 | 21.28 | 23.1 |
| Ca | 60.1 | 322.11 | 80.2 | 22.72 | 21.3 |
| Cb | 64.5 | 392.32 | 84.4 | 34.58 | 20.2 |
| Cc | 67.2 | 302.49 | 78.1 | 26.33 | 18.6 |

structures remained almost unchanged after more than 135 simulations using the same solvent. The difference in solvents causes the thermodynamic properties and kinetics of PVDF membrane systems to differ from one solvent system to another. The solvents mainly affect the structure and performance of PVDF membranes through the interaction coefficients between solvents/polymers, and thus, the structure and performance of PVDF membranes.[47]

The results of the electron microscopy experiments in Figure 8 are consistent with the simulations. When DMF is used as the solvent, the surface of the membrane is the densest, the cross-sectional structure shows a cell-cavity sponge structure, and the membrane pore connectivity is poor. When DMAc is used as the solvent, the surface of the membrane shows a granular microporous structure relative to DMF. The surface of the membrane is denser, the pore diameter is moderate, the number of pores is more uniformly distributed, the cross-section shows a finger-like pore structure, and the connectivity of the membrane pores is good. When DMSO is used as the solvent, the number of holes on the surface is large and unevenly distributed, the finger holes are wider, some of them are connected up and down, and there are aggregated PVDF spherical crystals in the lower part of the membrane with the highest porosity.

The structures and properties of the blended membranes are completely inconsistent because of the separate thermodynamic and kinetic controls of the film formation process. The link between the thermodynamic and membrane properties is small, whereas the link between the kinetic factors and the membrane structure is large. Different solution systems are controlled by different phase-separation behaviors. Although the phase-separation behavior is influenced by both thermodynamics and kinetics, the generation of picosublayers is related to both factors.

## 5. CONCLUSIONS

The simulation results were compared to the experimental results to illustrate the specific application of the ternary membrane system in a phase-field simulation. The following conclusions were drawn.

(1) The simulation results were in agreement with the experimental results, which verified the validity and accuracy of the model. Therefore, the mathematical model can be applied to ternary membrane systems by modifying specific chemical parameters, which has a certain guiding significance for predicting the development of the structure and performance of the blended membrane. This expands the application of the Cahn–Hilliard equation in the field of polymer phase transformation and realizes the ternary treatment of quaternary substances by combining solvents and additives, which enriches the quaternary substance treatment method.

(2) According to the simulation and experimental results, using water-soluble polymers (PEG and PVP) as additives led to the phase separation of the skin layer from the liquid–solid phase to the predominantly liquid–liquid phase with an increase in additive concentration and delay time ($t_1$). Subsequently, the

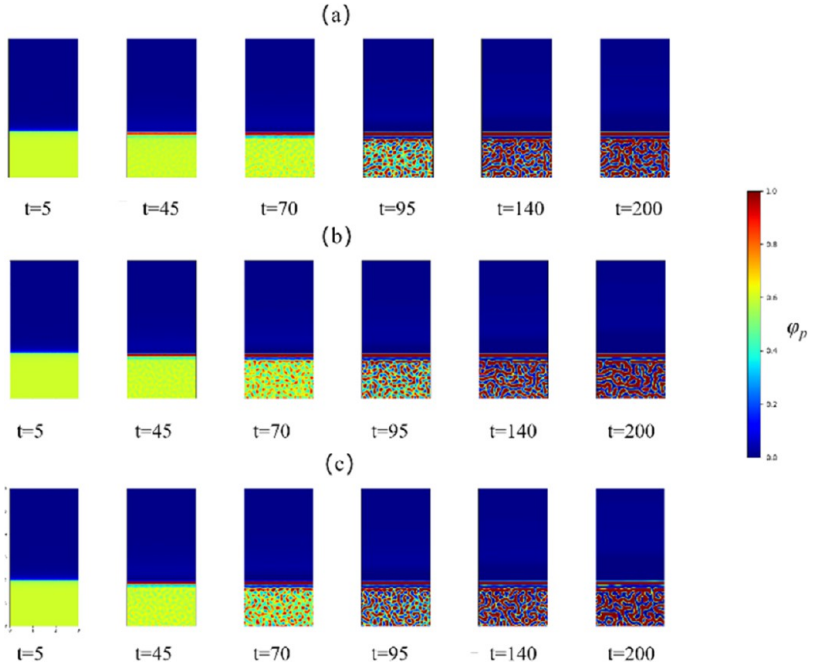


**Figure 7.** Microsimulation of the quaternary PVDF membrane system when the volume fraction of PVDF is 18% and the solvents are DMF (a), DMAC (b), and DMSO (c).



https://doi.org/10.1021/acsomega.3c09274
ACS Omega 2024, 9, 19911–19922

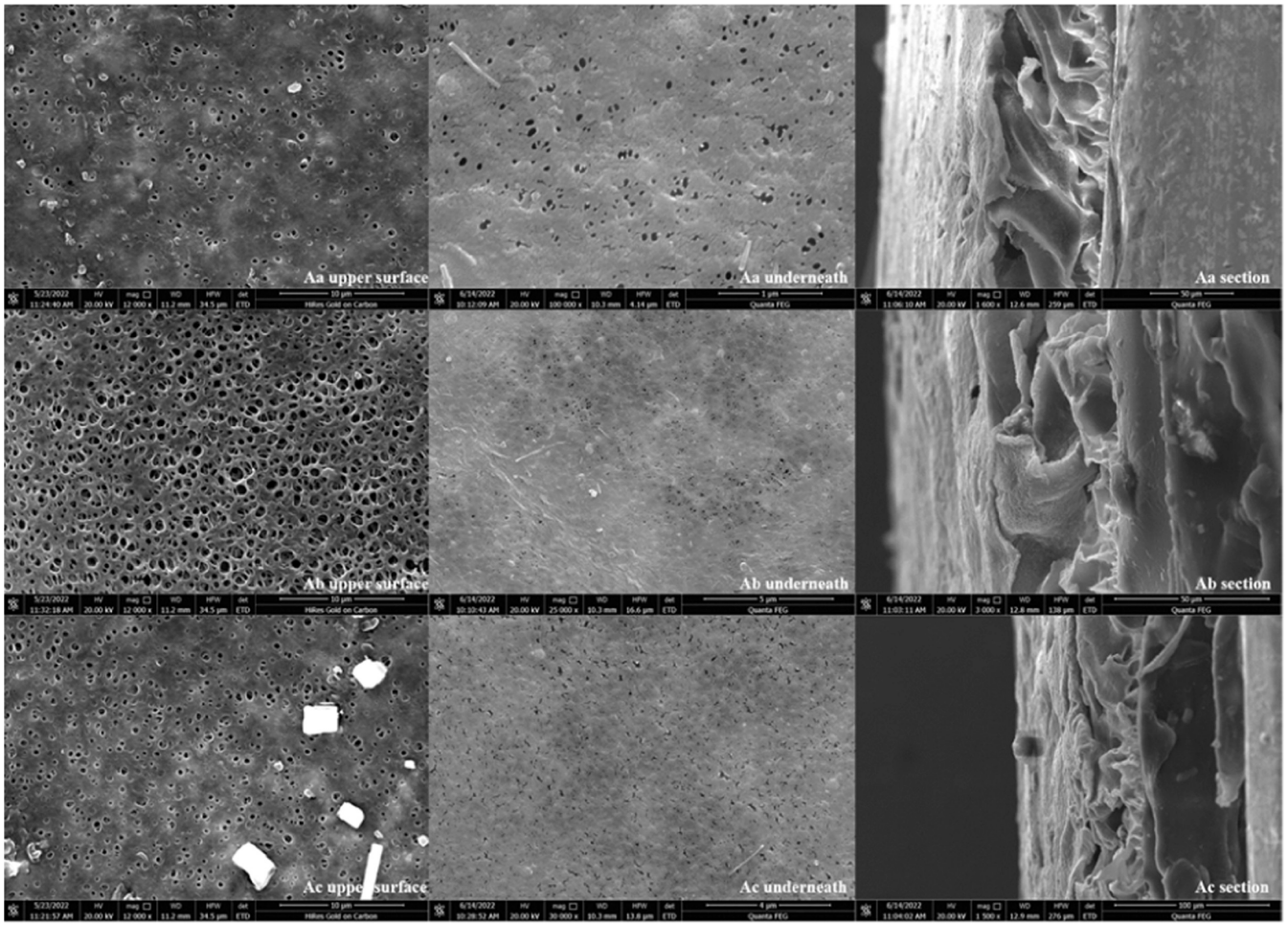


**Figure 8.** Electron microscopy images of membrane pairs with different solvents: (a) DMF, (b) DMAC, and (c) DMSO.

delay time of the skin layer increased, the skin layer became thicker and denser, and the viscosity of the whole system increased. The precipitation rate of the casting liquid slowed down, and the inflection point in the performance and structure of the membrane was observed. Moreover, the pore size on the surface and the development of large pores within the membrane first increased and then decreased; the porosity of the membrane, the water flux, and the degree of crystallinity first increased and then decreased with the increase in the concentration of additives. This phenomenon was also observed in the simulation. Hence, low concentrations of polymer additives promote pore generation, while high concentrations of polymer additives inhibit pore generation.

(3) DMAc, DMF, and DMSO were used for investigating the effects of different solvents on the structure and properties of the blended films. The thermodynamic properties of the three systems were as follows: the most stable was the DMAc solvent system, and the least stable was the DMSO solvent system. The phase-separation type of the membranes changed from transient phase separation to delayed phase separation in the order of the solvent systems DMSO, DMAc, and DMF, and the structure of the membranes changed from a porous to a dense membrane structure. Among them, DMSO showed the best development of macropores in the membrane, indicating a porous structure with large pores running through it, whereas DMAc and DMF exhibited dense granular structures.

The current model can be applied to quaternary PVDF membrane systems for simulating the membrane formation process during the submerged precipitation phase transition. However, in actual membrane production, one often chooses to modify the blended membrane by mixing solvents, adding more additives, adding ions to the gel bath, etc. The model will continue to be deepened in the future.

## AUTHOR INFORMATION

### Corresponding Author

**Ping Fang** − *School of Urban Planning and Municipal Engineering, Xi'an Polytechnic University, Xi'an 710600, People's Republic of China;* orcid.org/0000-0003-2765-1383; Email: 469493@qq.com

### Authors

**Zhuang Zhang** − *School of Urban Planning and Municipal Engineering, Xi'an Polytechnic University, Xi'an 710600, People's Republic of China;* orcid.org/0009-0009-1733-4297

**Yumeng Jiang** − *School of Urban Planning and Municipal Engineering, Xi'an Polytechnic University, Xi'an 710600, People's Republic of China*



https://doi.org/10.1021/acsomega.3c09274
*ACS Omega* 2024, 9, 19911−19922

**Shurong Cui** − *School of Urban Planning and Municipal Engineering, Xi'an Polytechnic University, Xi'an 710600, People's Republic of China*

**Chaoyu Yang** − *School of Urban Planning and Municipal Engineering, Xi'an Polytechnic University, Xi'an 710600, People's Republic of China;* orcid.org/0000-0001-8758-8852

Complete contact information is available at: https://pubs.acs.org/10.1021/acsomega.3c09274

### Notes

The authors declare no competing financial interest.

## ■ ACKNOWLEDGMENTS

The authors acknowledge the School of Urban Planning and Municipal Engineering of Xi'an Polytechnic University for providing experimental equipment and the Xi'an Municipal Science and Technology Project, China (23GXFW0023). The authors would also like to acknowledge the mentors of the Changqing Oil Field Company and Xi'an Polytechnic University for their guidance and insight into the direction of the project.

## ■ REFERENCES

(1) Zuo, D. Y. Structural Control and Properties of PVDF Microporous Membranes Prepared by Solution Phase Transition Method. Ph.D. Thesis, Zhejiang University, 2006.

(2) Mulder, M. *Basic Principle of Membrane Technology*; Kluwer: Academic, 1992; pp 1−109.

(3) Van De Witte, P.; Dijkstra, P.; Van Den Berg, J.; Feijen, J. Phase separation processes in polymer solutions in relation to membrane formation. *J. Membr. Sci.* **1996**, *117*, 1−31.

(4) Fujii, Y.; Iwatani, H.; Kigoshi, S. Morphological structures of the membranes prepared from polymer solutions. *Polym. J.* **1992**, *24*, 737−755.

(5) Lu, X.; Bian, X. Research on the modification and application of ultrafiltration membrane. *Membr. Sci. Technol.* **2003**, *23* (115), 97−102.

(6) Cohen, C.; Tanny, G.; Prager, S. Diffusion-controlled formation of porous structures in ternary polymer systems. *J. Polym. Sci.* **1979**, *17*, 477−489.

(7) Yilmaz, L.; McHugh, A. Analysis of nonsolvent-solvent-polymer phase diagrams and their relevance to membrane formation modeling. *J. Appl. Polym. Sci.* **1986**, *31*, 2847.

(8) Yilmaz, L.; Mchugh, A. Modelling of asymmetric membrane formation. I. Critique of evaporation models and development of a diffusion equation formalism for the quench period. *J. Membr. Sci.* **1986**, *28*, 287−310.

(9) Cheng, L. P.; Soh, Y. S.; Dwan, A. H.; Gryte, C. C. An improved model for mass transfer during the formation of polymeric membranes by the immersion-precipitation process. *J. Polym. Sci., Part B: Polym. Phys.* **1994**, *32*, 1413−1425.

(10) Zhou, B.; Powell, A. C. Phase field simulations of early stage structure formation during immersion precipitation of polymeric membranes in 2D and 3D. *J. Membr. Sci.* **2006**, *268*, 150−164.

(11) Zhang, L.; Shi, Y.; Wang, T.; Li, S.; Zheng, X.; Zhao, Z.; Feng, Y.; Zhao, Z. Fabrication of novel anti-fouling poly (m-phenylene isophthalamide) ultrafiltration membrane modified with Pluronic F127 via coupling phase inversion and surface segregation. *Sep. Purif. Technol.* **2022**, *282*, No. 120106, DOI: 10.1016/j.seppur.2021.120106.

(12) Pan, Y.; Yang, Y. X.; Chang, N.; Wang, Z.; Guan, W.; Yang, J. Z. A new theoretical model-The ionic molar surface Gibbs free energy and its application. *J. Chem. Thermodyn.* **2018**, *116*, 107−113.

(13) Wu, N.; Ji, X.; An, R.; Liu, C.; Lu, X. Generalized Gibbs free energy of confined nanoparticles. *AIChE J.* **2017**, *63*, 4595−4603.

(14) Li, M.; Stingelin, N.; Michels, J. J.; Spijkman, M. J.; Asadi, K.; Feldman, K.; Blom, P. W.; De Leeuw, D. M. Ferroelectric phase diagram of PVDF: PMMA. *Macromolecules* **2012**, *45*, 7477−7485.

(15) Chakraborty, J. Phase transformation in ultra-thin films. *Adv. Mater. Res.* **2014**, *996*, 860−865.

(16) Cahn, J. W.; Hilliard, J. E. Free energy of a nonuniform system. I. Interfacial free energy. *J. Chem. Phys.* **1958**, *28*, 258−267.

(17) Abe, T. Thermal equilibrium concentration fluctuations above the critical temperature in a Ni— Cu alloy. *Acta Metall. Mater.* **1992**, *40*, 1951−1959.

(18) Onsager, L. Reciprocal relations in irreversible processes. II. *Phys. Rev.* **1931**, *38*, 2265−2279.

(19) Barton, B. F.; Graham, P.; Mchugh, A. Dynamics of spinodal decomposition in polymer solutions near a glass transition. *Macromolecules* **1998**, *31*, 1672−1679.

(20) Cappelezzo, M.; Capellari, C.; Pezzin, S.; Coelho, L. Stokes-Einstein relation for pure simple fluids. *J. Chem. Phys.* **2007**, *126*, No. 224516, DOI: 10.1063/1.2738063.

(21) Harris, K. R. Communications: the fractional Stokes-Einstein equation: application to water. *J. Chem. Phys.* **2010**, *132*, No. 231103, DOI: 10.1063/1.3455342.

(22) Miller, C. C. The Stokes-Einstein law for diffusion in solution. *Proc. R. Soc. London, Ser. A* **1924**, *106*, 724−749.

(23) Vatin, M.; Duvail, M.; Guilbaud, P.; Dufrêche, J. F. Liquid/liquid interface in periodic boundary condition. *Phys. Chem. Chem. Phys.* **2021**, *23*, 1178−1187.

(24) Iwata, M.; Ishibashi, Y. Lattice Vibrations in Finite Discrete Systems with Symmetric and Asymmetric Boundary Conditions. *Ferroelectrics* **2012**, *433*, 12−21.

(25) Planková, B.; Lísal, M. Molecular dynamics of aqueous salt solutions in clay nanopores under the thermodynamic conditions of hydraulic fracturing: Interplay between solution structure and molecular diffusion. *Fluid Phase Equilib.* **2020**, *505*, No. 112355, DOI: 10.1016/j.fluid.2019.112355.

(26) O'Brien, R.; Quon, D.; Darsi, C. Estimation of Molecular Diffusivities in Liquids. *J. Electrochem. Soc.* **1970**, *117*, 888−893.

(27) Burman, E.; Nechita, M.; Oksanen, L. A stabilized finite element method for inverse problems subject to the convection-diffusion equation. I: diffusion-dominated regime. *Numer. Math.* **2020**, *144*, 451−477.

(28) Xie, Y. High-Precision Parallel Algorithm for Concentration-Convection-Diffusion Equation and its Application. Ph.D Thesis, Dalian Maritime University, 2020.

(29) Li, X.; Gao, X. Evaluation of the effectiveness of dimensionless methods. *Stat. Decis. Making* **2021**, *37*, 24−28.

(30) Yue, L.; Xu, K.; Shi, G. Property analysis and method selection of the indexes being dimensionless. *J. Stat. Inf.* **2020**, *35*, 3−9.

(31) Agarwal, J. R.; Torres, C. F.; Shah, S. Development of dimensionless parameters and groups of heat and mass transfer to predict wax deposition in crude oil pipelines. *ACS Omega* **2021**, *6*, 10578−10591.

(32) Wang, Y.; Cakmak, M. Hierarchical structure gradients developed in injection-molded PVDF and PVDF-PMMA blends. I. Optical and thermal analysis. *J. Appl. Polym. Sci.* **1998**, *68*, 909−926.

(33) Nakagawa, K.; Ishida, Y. Annealing effects in poly (vinylidene fluoride) as revealed by specific volume measurements, differential scanning calorimetry, and electron microscopy. *J. Polym. Sci.* **1973**, *11*, 2153−2171.

(34) Saxena, R.; Caneba, G. T. Studies of spinodal decomposition in a ternary polymer-solvent-nonsolvent system. *Polym. Eng. Sci.* **2002**, *42*, 1019−1031.

(35) Jung, B.; Yoon, J. K.; Kim, B.; Rhee, H. W. Effect of molecular weight of polymeric additives on formation, permeation properties and hypochlorite treatment of asymmetric polyacrylonitrile membranes. *J. Membr. Sci.* **2004**, *243*, 45−57.

(36) Ahmad, T.; Guria, C.; Mandal, A. A review of oily wastewater treatment using ultrafiltration membrane: A parametric study to enhance the membrane performance. *J. Water Process. Eng.* **2020**, *36*, No. 101289.

(37) Ahmad, T.; Guria, C.; Mandal, A. Optimal synthesis and operation of low-cost polyvinyl chloride/bentonite ultrafiltration membranes for the purification of oilfield produced water. *J. Membr. Sci.* **2018**, *564*, 859−877.
(38) Moideen K, I.; Isloor, A. M.; Ismail, A.; Obaid, A.; Fun, H. K. Fabrication and characterization of new PSF/PPSU UF blend membrane for heavy metal rejection. *Desalin. Water Treat.* **2016**, *57*, 19810−19819.
(39) Samari, M.; Zinadini, S.; Zinatizadeh, A. A.; Jafarzadeh, M.; Gholami, F. Oily wastewater treatment using modified microfiltration membrane. *J. Appl. Res. Water Wastewater* **2020**, *7*, 97−101.
(40) Cai, R.; Zhou, Y.; Hu, J.; Lu, J.; Fan, X.; Chen, Y.; Ding, M.; Rong, J.; Liu, W.; Chen, Y. A novel sodium alginate/cellulose nanofiber self-supported hydrogel membrane and its filtration performance. *J. Water Process. Eng.* **2022**, *50*, No. 103303.
(41) Asadi, A.; Gholami, F.; Zinatizadeh, A. A.; Jaberi, H. Application of high hydrophilic antifouling nanofiltration membranes embedded with mesoporous carbon based nanoparticles for efficient dye removal and salt rejection 2021.
(42) Yu, Z.; Liu, X.; Zhao, F.; Liang, X.; Tian, Y. Fabrication of a low-cost nano-SiO2/PVC composite ultrafiltration membrane and its antifouling performance. *J. Appl. Polym. Sci.* **2015**, *132*, No. 41267, DOI: 10.1002/app.41267.
(43) Boom, R.; Wienk, I.; Van Den Boomgaard, T.; Smolders, C. Microstructures in phase inversion membranes. Part 2. The role of a polymeric additive. *J. Membr. Sci.* **1992**, *73*, 277−292.
(44) Han, M. J.; Nam, S. T. Thermodynamic and rheological variation in polysulfone solution by PVP and its effect in the preparation of phase inversion membrane. *J. Membr. Sci.* **2002**, *202*, 55−61.
(45) Fang, P.; Yang, C.; Shao, R.; Zhou, L.; Liu, K. Ternary phase-field simulations of the skin-sublayer structures in poly (vinylidene fluoride) microporous membranes prepared by a nonsolvent-induced phase separation. *ACS Omega* **2021**, *6*, 7444−7453.
(46) Fang, P.; Cui, S.; Song, Z.; Zhu, L.; Du, M.; Yang, C. Phase-Field Simulation of the Effect of Coagulation Bath Temperature on the Structure and Properties of Polyvinylidene Fluoride Microporous Membranes Prepared by a Nonsolvent-Induced Phase Separation. *ACS Omega* **2023**, *8*, 180−189.
(47) Dong, W.; Hakukawa, H.; Yamahira, N.; Li, Y.; Horiuchi, S. Mechanism of reactive compatibilization of PLLA/PVDF blends investigated by scanning transmission electron microscopy with energy-dispersive X-ray spectrometry and electron energy loss spectroscopy. *Acs. Appl. Polym. Mater.* **2019**, *1*, 815−824.


https://doi.org/10.1021/acsomega.3c09274
*ACS Omega* 2024, 9, 19911−19922